

Mutations of the Serine Protease *CAP1/Prss8* Lead to Reduced Embryonic Viability, Skin Defects, and Decreased ENaC Activity

Simona Frateschi,* Anna Keppner,*
Sumedha Malsure,* Justyna Iwaszkiewicz,[†]
Chloé Sergi,* Anne-Marie Merillat,*
Nicole Fowler-Jaeger,* Nadia Randrianarison,[‡]
Carole Planès,[‡] and Edith Hummler*

From the Department of Pharmacology and Toxicology* and the Protein Modeling Facility,[†] University of Lausanne, Lausanne, Switzerland; and Equipe d'Accueil EA 2363 Cellular and Functional Responses to Hypoxia,[‡] UFR Health, Medicine and Human Biology - Bobigny, Paris University 13, Paris, France

CAP1/Prss8 is a membrane-bound serine protease involved in the regulation of several different effectors, such as the epithelial sodium channel ENaC, the protease-activated receptor PAR2, the tight junction proteins, and the profilaggrin polypeptide. Recently, the V170D and the G54-P57 deletion mutations within the CAP1/Prss8 gene, identified in mouse frizzy (*fr*) and rat hairless (*fr^{CR}*) animals, respectively, have been proposed to be responsible for their skin phenotypes. In the present study, we analyzed those mutations, revealing a change in the protein structure, a modification of the glycosylation state, and an overall reduction in the activation of ENaC of the two mutant proteins. *In vivo* analyses demonstrated that both *fr* and *fr^{CR}* mutant animals present analogous reduction of embryonic viability, similar histologic aberrations at the level of the skin, and a significant decrease in the activity of ENaC in the distal colon compared with their control littermates. Hairless rats additionally had dehydration defects in skin and intestine and significant reduction in the body weight. In conclusion, we provided molecular and functional evidence that CAP1/Prss8 mutations are accountable for the defects in *fr* and *fr^{CR}* animals, and we furthermore demonstrate a decreased function of the CAP1/Prss8 mutant proteins. Therefore, *fr* and *fr^{CR}* animals are suitable models to investigate the consequences of CAP1/Prss8 action on its target proteins in the whole organism. (Am J Pathol 2012, 181:605–615; <http://dx.doi.org/10.1016/j.ajpath.2012.05.007>)

Proteolytic enzymes and their inhibitors count for >2% of the known proteome, and a crucial role of these proteins in tissue homeostasis, diseases, and development has been demonstrated.^{1–4}

CAP1/Prss8 (also known as prostaticin) is a glycosylphosphatidylinositol membrane-anchored serine protease expressed in the epithelium of various organs, such as prostate, kidney, lung, colon, and skin.^{5–7} CAP1/Prss8 was the first of several membrane-tethered serine proteases found to activate the amiloride-sensitive epithelial sodium channel ENaC in a kidney epithelial cell line, and for this reason it was named channel-activating protease 1 (CAP1).^{8,9} These findings predicted that CAP1/Prss8 has an important role in regulating the epithelial sodium transport *in vivo*,¹⁰ and ENaC currents became a suitable way to monitor CAP1/Prss8 activity.

CAP1/Prss8 has also been demonstrated to play essential functions in the physiopathology of lung and skin. CAP1/Prss8 inactivation addressed to the alveolar epithelium decreased ENaC-mediated alveolar sodium transport and increased alveolar lining fluid volume in an experimental model of acute volume overload.⁶ The lack of CAP1/Prss8 in the skin caused early postnatal mortality because of severe skin dehydration defects, altered the processing of profilaggrin and generating defective tight junctions.⁷ On the other hand, CAP1/Prss8 overexpression in the skin severely impaired the epidermal barrier function and provoked ichthyosis and inflammation. Those pathologic features were completely negated when superposed on a protease-activated receptor 2 (PAR2) knockout background, placing PAR2 as a downstream effector of CAP1/Prss8.¹ PAR2 is a G-protein-coupled receptor also involved in neural tube closure, and it can be activated by local proteases as CAP1/Prss8 for regulating epithelial integrity.¹¹ Moreover, CAP1/Prss8

Supported by the Swiss National Science Foundation (grant 3100A0-102125/1 to E.H.), the Swiss National Centre of Competence in Research Kidney Control of Homeostasis, and the Leducq Fondation.

Accepted for publication May 2, 2012.

Address reprint requests to Edith Hummler, Ph.D., Département de Pharmacologie et de Toxicologie, Rue du Bugnon 27, CH-1005 Lausanne, Switzerland. E-mail: Edith.Hummler@unil.ch.

was found to be down-regulated in hormone refractory prostate cancers, gastric cancer, and breast cancer^{12–14} and up-regulated in epithelial ovarian cancer,¹⁵ suggesting an additional role of CAP1/Prss8 in tumor invasion. Thus, CAP1/Prss8 emerged as involved in various different processes that range from organ integrity to disease.

Recently, Spacek and colleagues¹⁶ located the genetic defects in the spontaneous mouse frizzy (*fr*) and rat hairless (*fr^{CR}*) models on the *CAP1/Prss8* gene.¹⁶ Mice carrying the *fr* mutation in homozygosity display a nearly normal, wavy coat and distinctly curly vibrissae that are apparent after birth and persist throughout life.¹⁷ The Charles River *fr^{CR}* rat is one of the autosomal recessive hypotrichotic models actively studied in pharmacologic and dermatologic research, and it is characterized by almost complete baldness.¹⁸ Spacek and coworkers demonstrated that the *fr* mutation consists of a T to A transversion in the *CAP1/Prss8* gene that results in a valine to aspartate substitution at residue 170. The assignment of *fr* mutation on the *CAP1/Prss8* gene was supported by complementation test that indicated the failure of the knockout allele (Δ) of *CAP1/Prss8*¹⁹ to complement the *fr* defect in compound heterozygotes (*fr*/ Δ). In addition, sequence analysis of *CAP1/Prss8* coding regions in *fr^{CR}* rat identified a 12-bp deletion in the third exon, leading to G54-P57 ablation in the *CAP1/Prss8* protein, which indicated that *fr* and *fr^{CR}* mutations may indeed be orthologues,¹⁶ as already suggested by previous studies.²⁰ Therefore, the V170D missense and G54-P57 deletion mutations in the *CAP1/Prss8* gene have been proposed as the molecular bases for the *fr* and *fr^{CR}* variants, respectively.

Aiming to investigate whether these genetic data could be supported by molecular and functional evidence, we analyzed the consequences of those mutations and performed *in silico*, *in vitro*, and *in vivo* experiments. V170D and G54-P57 deletion mutations changed *CAP1/Prss8* protein structure and reduced ENaC activation in the *Xenopus laevis* oocyte cell system. Inheritance, histologic, and functional studies of *fr/fr* mice, *fr*/ Δ mice, and *fr^{CR}/fr^{CR}* rats compared with littermate control groups, unveiled very similar features among these variants, defined by reduced embryonic viability, skin abnormalities, and decreased ENaC activity in the distal colon. Therefore, we could demonstrate, at the molecular and functional level, that the *fr* and *fr^{CR}* phenotypes are caused by V170D and G54-P57 deletion mutations in the *CAP1/Prss8* gene. Finally, *fr* and *fr^{CR}* animals emerged as suitable models for *CAP1/Prss8* reduced function in the whole organism.

Materials and Methods

Homology Modeling, *in Silico* Alanine Scanning, and Amino Acid Alignment

Mouse *CAP1/Prss8* 45–290 sequence fragment obtained from the *CAP1/Prss8* entry Q9ESD1 at the UniProt knowledgebase²¹ was a target sequence for homology modeling of murine *CAP1/Prss8* structure. As a template, the crystal structure of human homologous protein available

in the protein structures database under the 3DFJ code was used.²² The alignment between the two sequences was built using the Modeller 9v5 program (http://sallib.org/modeller/download_installation.html).²³ An 80% sequence identity between the target and the template sequence in the calculated alignment implies a good reliability of the final model. The standard modeling procedure using spatial restraints derived from the alignment was performed with the Modeler 9v5 program. The 100 models were constructed, and their ANOLEA scores²⁴ were calculated. The model with the best overall ANOLEA score was chosen for further studies. The quality of the model was checked with the PROCHECK software (<http://www.ebi.ac.uk/thornton-srv/software/PROCHECK>) and PDBsum software (<http://www.ebi.ac.uk/thornton-srv/databases/pdbsum/Generate.html>). Noteworthy, no residues were appearing in the disallowed regions of Ramachandran plot, and 91.1% of residues appeared in the most favored regions of the plot, indicating the good quality of the structure. The FoldX program (<http://foldx.crg.es>)²⁵ was used to perform a computational alanine scan by mutating selected residues to an alanine and estimating the change in the protein stability. Amino acid alignment was performed by using the clustalw2 program (<http://www.ebi.ac.uk/Tools/msa/clustalw2>; EMBL-EBI Wellcome Trust Genome Campus Hinxton, Cambridgeshire, UK).

Construct Preparation, *Xenopus* Oocyte Injections, Electrophysiologic Measurements, and HEK-293 Cell Transfections

The T to A transversion that results in a valine to aspartate substitution at residue 170 and the 5'-GGTCAGTG-GCCC-3' deletion that results in G54-P57 ablation in the transcribed protein were each inserted into the mouse *CAP1/Prss8* coding sequence (GenBank GenInfo Identifier 19111159) and introduced in the pSDeasy expression vector, a modified pSD5 vector,²⁶ for *in vitro* transcription. SP6 RNA polymerase (Promega, Madison, WI) was used for cRNA synthesis.

Expression studies performed in *X. laevis* oocytes (African *Xenopus* Facility, Noordhoek, South Africa) in stage V/VI have been previously described.²⁷ A total of 0.25 ng of each cRNA encoding the three rat ENaC subunits in the presence or absence of 2 ng of wild-type (WT) or mutant *CAP1/Prss8* cRNA in a total volume of 50 nL was injected into oocytes. Oocytes were incubated in modified Barth saline solution. Twenty-four hours after cRNA injection, electrophysiologic measurements were performed using the two-electrode voltage clamp technique. The amiloride-sensitive current was measured in the presence of 120 mmol/L Na⁺ in frog Ringer with and without 5 μ mol/L amiloride and without 20 mg/mL of trypsin at a holding potential of -80 mV.

WT and mutant mouse *CAP1/Prss8* coding sequences were inserted in the pRK5 expression vector for HEK-293 cells transfection. HEK-293 were cultured in Dulbecco's modified Eagle's medium (DMEM) supplemented with 10% fetal calf serum and 100 μ g/mL gentamicin and

transfected at 50% to 60% confluence in 100-mm dishes using the calcium-phosphate method. After transfection, cells were grown for 48 hours in DMEM supplemented with 10% fetal calf serum before harvesting. The total amount of transfected DNA was 12 μg per 100-mm dish.

Western Blot and Pulse-Chase Experiments

Xenopus oocytes were homogenized in 1% Triton X-100, 20 mmol/L Tris-HCl, pH 7.6, and 100 mmol/L NaCl. Lysates were centrifuged at $13,000 \times g$ for 10 minutes at 4°C. HEK-293 cells were lysed using 1 mL of lysis buffer per dish of 1% Triton buffer (20 mmol/L Tris-HCl, pH 7.4, 150 mmol/L NaCl, 1% Triton X-100, 100 mmol/L each leupeptin, pepstatin, and aprotinin, 10 mmol/L phenylmethylsulfonyl fluoride). HEK-293 cells lysates were incubated 1 hour at 4°C on a rotating wheel. The solubilized material was centrifuged at $10,000 \times g$ for 30 minutes at 4°C, and the supernatants were collected. Animal tissues were lysed in 1 mL of radioimmunoprecipitation assay buffer (50 mmol/L Tris-HCl, pH 7.2, 150 mmol/L NaCl, 1% NP-40, 0.1% SDS, 0.5% sodium deoxycholate, 100 mmol/L each leupeptin, pepstatin, and aprotinin, 10 mmol/L phenylmethylsulfonyl fluoride). Lysates were centrifuged at $13,000 \times g$ for 15 minutes at 4°C, and the supernatants were collected. For SDS-PAGE, samples were loaded and separated on a 10% polyacrylamide gel. Western blot analysis was performed using rabbit anti-mouse antibodies to CAP1/Prss8.²⁸ Signals were revealed using anti-rabbit IgG from goat (1:10,000; GE Healthcare, Glattbrugg, Switzerland) as secondary antibody and the SuperSignal West Dura detection system (Pierce, Rockford, IL).

To study CAP1/Prss8 protein expression, cRNA-injected oocytes were incubated in modified Barth's solution (MBS) containing 0.7 to 1 mCi/mL [³⁵S]methionine (NEG772007MC; Perkin Elmer, Schwerzenbach, Switzerland) for 6 hours and subjected to 4- and 16-hour chase periods in MBS containing 10 mmol/L unlabeled methionine. After the pulse-chase periods, protein extracts were prepared and subjected to non-denaturing immunoprecipitations.²⁹ After overnight incubation at 4°C with CAP1/Prss8 antibody, the immune complexes were recovered on protein A Sepharose beads (GE Healthcare, Waukesha, WI) and washed several times with MBS containing unlabeled methionine. Immunoprecipitates were resolved by SDS-PAGE (10% polyacrylamide) gels.

Isolation of Rat AECs

The procedure of rat alveolar epithelial cell (AEC) isolation accorded with legislation currently in force in France and Switzerland and animal welfare guidelines (Ministère Français de la Pêche et de l'Agriculture, agreement 5669). The AECs were isolated from adult WT, heterozygous, and homozygous mutant rats by elastase digestion of lung tissue followed by sequential filtration and differential adherence on bacteriologic dishes as previously described.²⁸ Cell purity was >80%, and cell viability >95%.

Preparation of AEC Protein Extracts and Western Blotting Procedure

Freshly isolated rat AECs were resuspended in 30 μL of ice-cold lysis buffer containing 150 mmol/L NaCl, 50 mmol/L Tris-HCl, pH 7.6, 1% Triton X-100, 0.1% SDS, and protease inhibitors and kept on ice for 1 hour. Cell lysates were then centrifuged at $15,000 \times g$ for 15 minutes at 4°C, and samples of the supernatants were immediately frozen before use. For Western blotting, samples of protein extracts (40 μg total protein) in one volume of sample buffer (containing 13.8% sucrose, 9.6% SDS, 4.2% β -mercaptoethanol, and 0.0126% bromophenol blue in water) were resolved through 10% acrylamide gels, electrophoretically transferred to polyvinylidene difluoride membranes, and subsequently probed for CAP1 protein detection. The goat anti-rabbit IgG secondary antibody (Santa Cruz Biotechnology, Santa Cruz, CA) was used at dilution 1:3000, and the signal was developed with the Western Blotting Luminol Reagent (Santa Cruz Biotechnology).

Animal Genotyping and Stool Assay

The genotype of *fr* mouse and *fr*^{CR} rat animal models (kindly provided by Dr. Thomas R. King; Biomolecular Sciences, Central Connecticut State University, New Britain, CT) was assessed as formerly described.¹⁶ We previously reported the generation and genotyping of the engineered null allele (Δ) of CAP1/Prss8.¹⁹ Experimental procedures and animal maintenance followed federal guidelines and were approved by local authorities. All animals were housed in a temperature- and humidity-controlled room with an automatic 12-hour light/dark cycle and had free access to food and tap water.

Fecal hydration was assessed as follows: freshly evacuated stools were collected in the morning and weighed before and after at least 2 hours of dehydration performed by using the SpeedVac. Values are expressed as means \pm SEM of the difference in weight.

RNA Extraction and Quantitative RT-PCR

Cells and organs were homogenized using tissue lyser (Qiagen, Valencia, CA), and RNA was extracted with the Qiagen RNeasy Mini kit (Basel, Switzerland) following the manufacturer's instructions. A total of 1 μg of RNA was reverse-transcribed using M-MLV Reverse Transcriptase RNase H Minus Point Mutant (Promega AG, Dübendorf, Switzerland). Real-time PCR was performed by TaqMan PCR using Applied Biosystems 7500 (Carlsbad, CA). Each measurement was taken in duplicate. Quantification of fluorescence was normalized to β -actin. Primer and probe sequences have been previously described.¹

Immunofluorescence and Histologic Analysis

Cells and organs were embedded into paraffin. Slides were incubated in xylene for at least 4 hours and rinsed with decreasing concentrations of ethanol. Antigen retrieval was performed for 10 minutes in TEG buffer. Slides

were washed in 50 mmol/L NH_4Cl in PBS for 30 minutes and blocked by 1% bovine serum albumin, 0.2% gelatin, and 0.05% saponin in PBS at room temperature for 10 minutes three times. Primary antibody was diluted in 0.1% BSA, 0.3% Triton X-100 in PBS, overnight at 4°C. Affinity-purified CAP1/Prss8 rabbit anti-mouse antiserum²⁸ was diluted 1:200. Slides were rinsed three times for 10 minutes in PBS containing 0.1% bovine serum albumin, 0.2% gelatin, and 0.05% saponin at room temperature, and the secondary antibody (Alexa Fluor 488 diluted 1:5000; Invitrogen, Grand Island, NY) was diluted in 0.1% bovine serum albumin and 0.3% Triton X-100 in PBS. Staining was visualized using an LSM confocal microscope (LSM 510 Meta, Carl Zeiss MicroImaging Inc., Jena, Germany).

For H&E staining, the paraffin was removed and the slides rehydrated 2 times in xylol for 5 minutes, 2 times in 100% ethanol for 1 minute, in 95% ethanol for 1 minute, and finally with tap water. Slides were incubated in staining glychemalun solution (0.013 mol/L Hematein, Gurr #34036; 0.3133 mol/L potassium alum, Merck #1047; 30% glycerol; 1% acetic acid, Merck #1.00063) for 4 minutes, tap water, 1% acid alcohol for 3 seconds, tap water, water for 15 seconds plus a few drops of NH_3 , tap water, 0.2% erythrosine solution (0.0023 mol/L erythrosin, Merck #15936; 0.1% formaldehyde, Merck #4003) for 30 seconds, and finally tap water. Slides were then dehydrated by following steps from 70% ethanol to xylol and mounted (Eukitt, Hatfield, PA). Pictures were taken using an Axion HRC (Carl Zeiss MicroImaging Inc.).

Measurement of TEWL and Rectal Transepithelial PD

The rate of transepithelial water loss (TEWL) from the ventral aspect of the skin of preshaved, anesthetized animals was measured using a Tewameter TM210 (Courage and Khazaka, Koln, Germany). The mean \pm SEM results are given.

Rectal potential difference (PD) and amiloride-sensitive rectal PD were measured in the morning (10 AM to noon) and in the afternoon (4 PM to 6 PM) of two different days of the same week. Animals were anesthetized with an i.p. injection of 75 mg/g body weight of Ketalar (Park-Davis, Baar, Switzerland) and 2.3 mg/g body weight of Rompun (Bayer, Leverkusen, Germany) and placed on a heated table. A winged needle filled with isotonic saline was placed in the subcutaneous tissue of the back. A double-barreled pipette was prepared from borosilicate glass capillaries (1.0 mm OD/0.5 mm ID; Hilgerberg, Malsfeld, Germany) and pulled to an approximate 0.2-mm tip diameter. The first barrel was filled with isotonic saline buffered with 10 mmol/L Na^+ -HEPES (pH 7.2), and the second barrel was filled with the same solution containing 25 mmol/L amiloride. The tip of the double-barreled pipette was placed in the rectum approximately 3 to 5 mm from the skin margin. The electrical PD was measured between the first barrel and the subcutaneous needle, both connected to Ag/AgCl electrodes by means of plastic tubes filled with 3 mmol/L KCl in 2% agar. The rectal PD was monitored continuously by

a VCC600 electrometer (Physiological Instruments, San Diego, CA) connected to a chart recorder. After stabilization of the rectal PD for approximately 1 minute, 0.05 mL of saline solution was injected through the first barrel as a control maneuver, and the PD was recorded for another 30-second period. A similar volume of saline solution containing 25 mmol/L amiloride was injected through the second barrel of the pipette, and the PD was recorded for another 1 minute. The amiloride-sensitive PD was calculated as the difference between the PD recorded before and after the addition of amiloride.

Results

Reduced ENaC Activation of V170D and G54-P57 CAP1/Prss8 Deletion Mutant Proteins

Taking advantage of the *in silico* protein modeling technique, we built the homology model of the mouse CAP1/Prss8 (Figure 1A), using as a template the crystal structure-based homology model of human CAP1/Prss8.³⁰ V170 belongs to one of the β strands in the inside of the protein and is located in a hydrophobic environment. V170 makes hydrophobic contacts with the methyl groups of V256 and L191. The alanine scanning for V170 resulted in 2.4 Kcal loss of energy upon mutation to Ala. G54-P57 residues (Gly-Gln-Trp-Pro) in CAP1/Prss8 are found on the external surface of the molecule and therefore are solvent exposed. This fragment, which is deleted in the *fr^{CR}/fr^{CR}* mutant rats, contains the structurally important Trp56, leading to 4.5-Kcal loss in stability when mutated to Ala. Multiple sequence alignments illustrated that the mutated residues are conserved among different species (Figure 1B).

To investigate the consequences of the V170D and G54-P57 deletion mutations on CAP1/Prss8 expression and function, we introduced V170D and G54-P57 deletion mutations in the mouse CAP1/Prss8, inserted the cDNA sequences in the pSDeasy expression vector for *in vitro* transcription,²⁶ and co-injected CAP1/Prss8 and ENaC cRNA in the *Xenopus* oocytes. CAP1/Prss8 cRNA stability was estimated by real-time PCR, and no remarkable difference in the level of each V170D and G54-P57 deletion mutant versus WT CAP1/Prss8 was observed (data not shown). CAP1/Prss8 immunostaining was detected at the plasma membrane in oocytes that were injected with WT CAP1/Prss8, and equal results were obtained with V170D and G54-P57 deletion CAP1/Prss8 mutants (Figure 2A). Western blot analysis against CAP1/Prss8 evidenced the presence of two bands, of 37 and 40 kDa, that might correspond to two different glycosylation states of the protein and showed that the two mutant proteins can be translated as well as the WT (Figure 2B). Glycosylation of CAP1/Prss8 was assessed by treatment of oocyte extracts with the deglycosylating enzyme PNGase F that revealed the presence of a nonglycosylated (n) native form upon deglycosylation treatment. Thus, the two bands of 37 and 40 kDa most likely correspond to the core-glycosylated form (c), which is typical of newly synthesized proteins, and the fully glycosylated

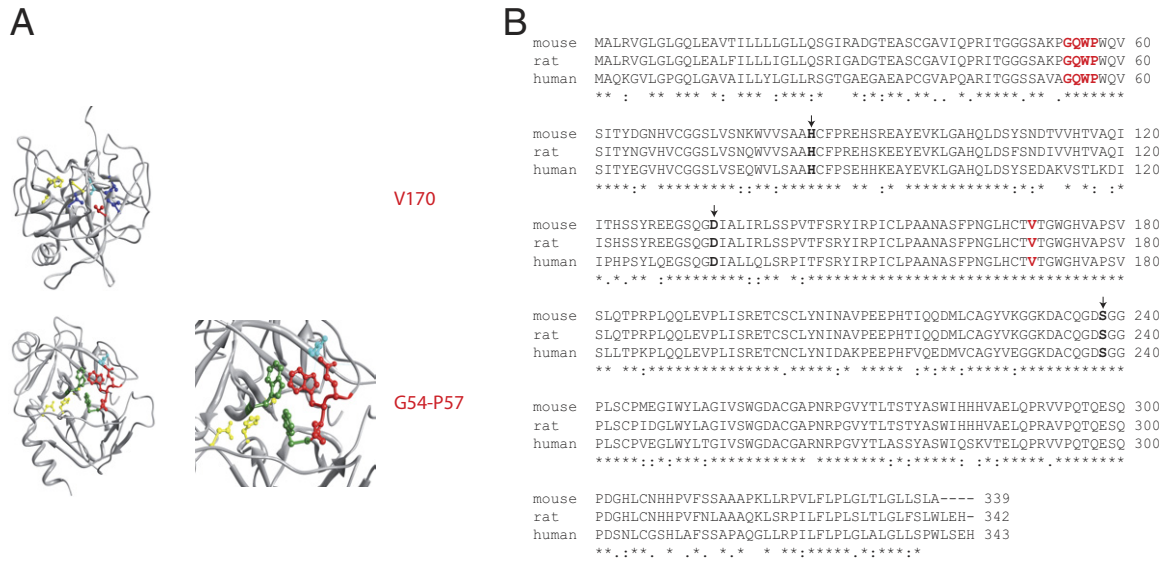


Figure 1. A: Homology model of the mouse CAP1/Prss8 tertiary protein structure constructed on the crystal structure–based homology model of the human CAP1/Prss8. Val170 residue, mutated into Asp in the *fr* mouse variant (**upper panels**, entire and zoomed view), and the Gly54–Gln–Trp–Pro57 fragment, deleted in the *fr^{CR}* rat variant (**lower panels**, entire and zoomed view), are highlighted in red. The residues of the serine protease active site, Asp134, His85, and Ser238, are represented in yellow. The hydrophobic environment of Val170 consists of Ile45, Leu191, and Val256 shown in dark blue and Asp237 in cyan. Gly54–Pro57 interacts with adjacent residues: Trp triad formed by Trp 56 (red) and Trp58 and Trp250 (in dark green), Gln190 (in cyan) side chain forming hydrogen bond with Trp56, and hydrogen bond formed by Gln55 and Lys52 backbone. **B:** Amino acid alignment of the full-length protein of mouse (GenInfo Identifier: 19111160), rat (GenInfo Identifier: 20301968), and human (GenInfo Identifier: 4506153) CAP1/Prss8 performed using the ClustalW2 multiple sequence alignment program (<http://www.ebi.ac.uk/Tools/msa/clustalw2>). Mouse and rat share 92% of CAP1/Prss8 sequence identity, mouse and human 77%, and rat and human 75%. The amino acids of the catalytic triad (His, Asp, Ser) are indicated by **arrows** and bold text. The four residues deleted in the *fr^{CR}* rat (Gly, Gln, Trp, Pro) and the Val170 substituted with Asp in the *fr* mouse variants are indicated in red and result conserved among these species. **Asterisks** indicate identical amino acid residues, and double dots and dots indicate amino acids with similar and less similar side chain properties, respectively.

form (f) characteristic of mature proteins, respectively (Figure 2C). Analogous results were obtained in transfected HEK-293 cells (Figure 2D).

To gain further insight not only into the production but also into the degradation of WT and mutant proteins, we performed pulse-chase experiments by pulsing radioactively the oocytes during 6 hours (P) and chasing them during 4 (C1) and 16 (C2) hours in unlabeled media. WT CAP1/Prss8 protein production was evident after 6 hours of pulse, and protein degradation was observed already after the first chase period. Similar results were obtained for the two mutant proteins. However, CAP1/Prss8 V170D and G54–P57 deletion mutants showed different glycosylation states compared with the WT CAP1/Prss8, evidencing an increased fully glycosylated state of the G54–P57 deletion mutant versus an increased core-glycosylated state of the V170D mutant (Figure 2E).

Co-expression of WT CAP1/Prss8 with ENaC leads to a significant increase in the amiloride-sensitive sodium current in the *Xenopus* oocyte cell system³¹; hence, ENaC current is considered an appropriate parameter to monitor CAP1/Prss8 activity. Trypsin can activate near-silent ENaC channels by significantly increasing its open probability, indicating maximal ENaC activity of the cells.³² Co-injection of WT CAP1/Prss8 and ENaC revealed a 3.7-fold significant increase in the amiloride-sensitive sodium current relative to trypsin compared with oocytes that were injected with ENaC alone. In contrast, when either CAP1/Prss8 V170D or G54–P57 deletion mutant was co-expressed with ENaC, the ability of CAP1/Prss8 to increase ENaC-mediated currents was significantly re-

duced, leading to a 2.8- and 2.1-fold increase relative to trypsin, respectively (Figure 2F).

Reduced Viability and Similar Hair Phenotype in *fr* Mouse and *fr^{CR}* Rat Models

To study the consequences of CAP1/Prss8 V170D and G54–P57 deletion mutations and to investigate whether they might be responsible for the phenotypes observed in the *fr* mouse and *fr^{CR}* rat models, we performed inheritance, histopathologic, molecular, and functional analyses of *fr/fr*, *fr/Δ*, and *fr^{CR}/fr^{CR}* versus control littermates.

Each *fr/fr* and *fr/Δ* mouse variant presented reduced prenatal viability, deriving from crosses of *fr/+* x *fr/Δ*, yielding only approximately 16% *fr/fr* and 13% *fr/Δ* mutant offspring, respectively, rather than the expected 25%. *fr^{CR}/+* x *fr^{CR}/+* rat crosses generated 10% *fr^{CR}/fr^{CR}* mutants instead of the expected 25%. A total of 83% of the *fr^{CR}/fr^{CR}* rats resulted in males (Tables 1 and 2).

The *fr/fr*, *fr/Δ*, and *fr^{CR}/fr^{CR}* animals were distinguishable from their siblings as soon as the hair started to grow. Compared with WT controls, *fr/fr* mice manifested curly whiskers and a wavy coat. The phenotype of *fr/Δ* animals was more severe, showing curly whiskers accompanied by less and shorter hair. *fr^{CR}/fr^{CR}* rats were almost completely bald. These data are in accordance with previous observations.^{16,20}

No histopathologic aberrations were observed in the lung, kidney, and distal colon. In contrast, *fr/fr* and *fr/Δ* mice and *fr^{CR}/fr^{CR}* rats presented hair bulbs deeply

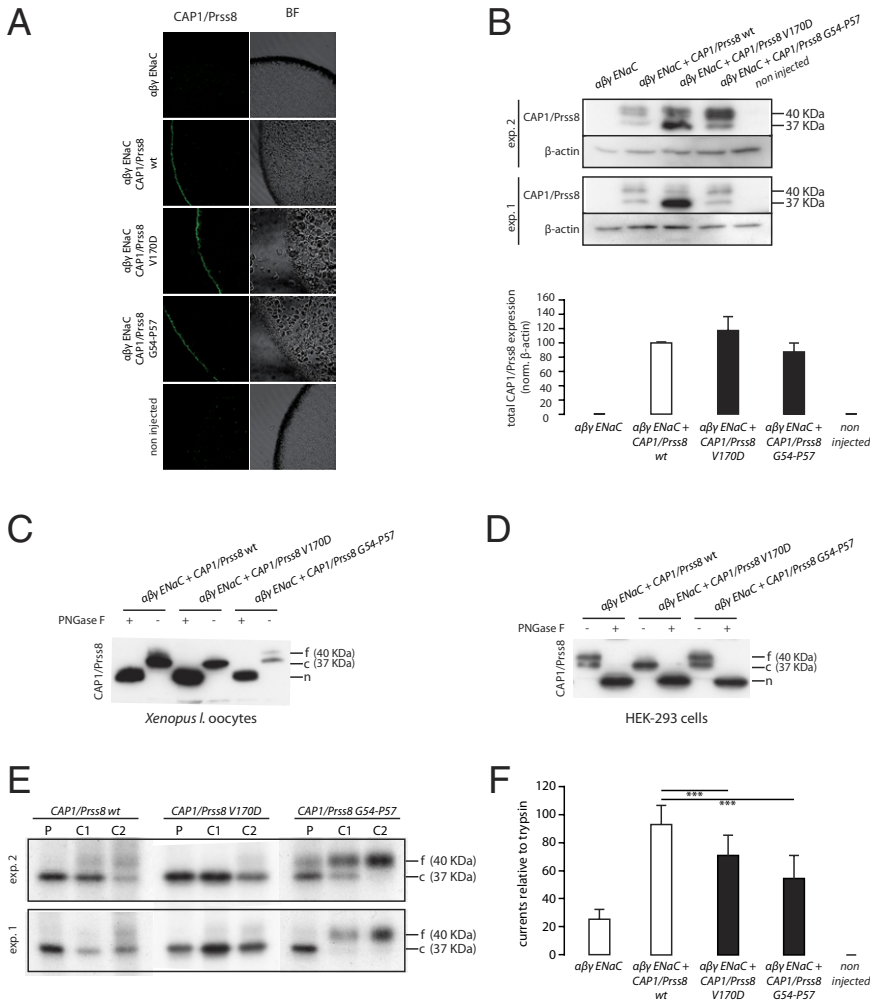


Figure 2. A: CAP1/Prss8 immunofluorescence (green) performed in *Xenopus* oocytes injected with ENaC and CAP1/Prss8 WT, V170D, and G54-P57 deletion mutant cRNA. BF, bright field. **B:** Oocytes were injected as indicated, and Western blot analyses were performed on cell lysates using CAP1/Prss8 and β -actin antibodies. Two representative experiments (exp. 1 and exp. 2) are shown, and quantification relative to β -actin was performed on a total of four independent experiments, each consisting of at least five oocytes injected per condition. **C:** Oocytes were injected as in B, and protein extracts were treated (+) or not (-) with PNGase F to deglycosylate the proteins and then subjected to Western blot analysis using CAP1/Prss8 antibody. f, fully glycosylated; c, core glycosylated; n, nonglycosylated. **D:** HEK-293 cells were transfected as indicated, and protein extracts were treated (+) or not (-) with PNGase F to deglycosylate the proteins and then subjected to Western blot analysis using CAP1/Prss8 antibody. This figure is representative of three independent experiments. **E:** Oocytes were injected as indicated and subjected to 6-hour pulse (P), 4-hour chase period (C1), and 16-hour chase period (C2). After the pulse-chase periods, protein extracts were prepared and subjected to nonreducing immune precipitations using CAP1/Prss8 antibody. Two experiments (exp. 1 and exp. 2) are shown and are representative of three independent experiments, each consisting of 15 oocytes injected per condition. **F:** Amiloride-sensitive sodium currents from four independent experiments pulled together, each consisting of at least five oocytes measured per condition before and after trypsin perfusion. The currents measured before the perfusion of the oocytes with trypsin were normalized to currents measured after trypsin perfusion. *** $P < 0.001$.

positioned in the lower dermis. In addition, *fr^{CR}/fr^{CR}* skin exhibited hyperplastic epidermis and hyperkeratosis, as well as swelled and more abundant sebaceous glands. Beside these structural and morphologic defects, no signs of inflammation, such as cellular infiltrations, were detectable in *fr/fr*, *fr/ Δ* , and *fr^{CR}/fr^{CR}* mutant skin (Figure 3).

Aiming to investigate CAP1/Prss8 expression at the transcriptional level, we performed quantitative real-time

PCR analyses on skin, lung, kidney, and colon extracts of *fr/fr* and *fr/ Δ* mutant mice and control littermates. For all analyzed organs, mice carrying $\Delta/+$ alleles presented a significant (50%) reduction in the expression of CAP1/Prss8 when compared with WT animals, as it might be predicted from the absence of one CAP1/Prss8 allele. Decreased CAP1/Prss8 expression was detected also in *fr/ Δ* heterozygous animals, but it was significant only in the kidney. CAP1/Prss8 mRNA levels in *fr/fr* mutants

Table 1. Inheritance of the *fr* and Δ Mutations

Breeding pair	<i>fr</i> and Δ genotype			
	+/+	<i>fr</i> /+	Δ /+	<i>fr</i> / Δ <i>fr</i> / <i>fr</i>
<i>fr</i> /+ x Δ /+ (n = 111)				
No. of animals	42	32	30	7
Observed, %	38	29	27	6
Expected, %	25	25	25	25
χ^2 test	21.3 ($P < 0.001$)			
<i>fr</i> / Δ x <i>fr</i> /+ (n = 95)				
No. of mutations		40	28	12 15
Observed, %		42	29	13 16
Expected, %		25	25	25 25
χ^2 test	22.0 ($P < 0.01$)			

Table 2. Inheritance of the *fr^{CR}* Mutations

Breeding pair	<i>fr^{CR}</i> genotype		
	+/+	<i>fr^{CR}</i> /+	<i>fr^{CR}</i> / <i>fr^{CR}</i>
<i>fr^{CR}</i> /+ x <i>fr^{CR}</i> /+ (n = 60)			
No. of animals	12	42	6
Observed, %	20	70	10
Expected, %	25	50	25
χ^2 test	18.0 ($P < 0.01$)		
<i>fr^{CR}</i> /+ x <i>fr^{CR}</i> / <i>fr^{CR}</i> (n = 50)			
No. of mutations		32	18
Observed, %		64	36
Expected, %		50	50
χ^2 test	7.8 ($P < 0.01$)		

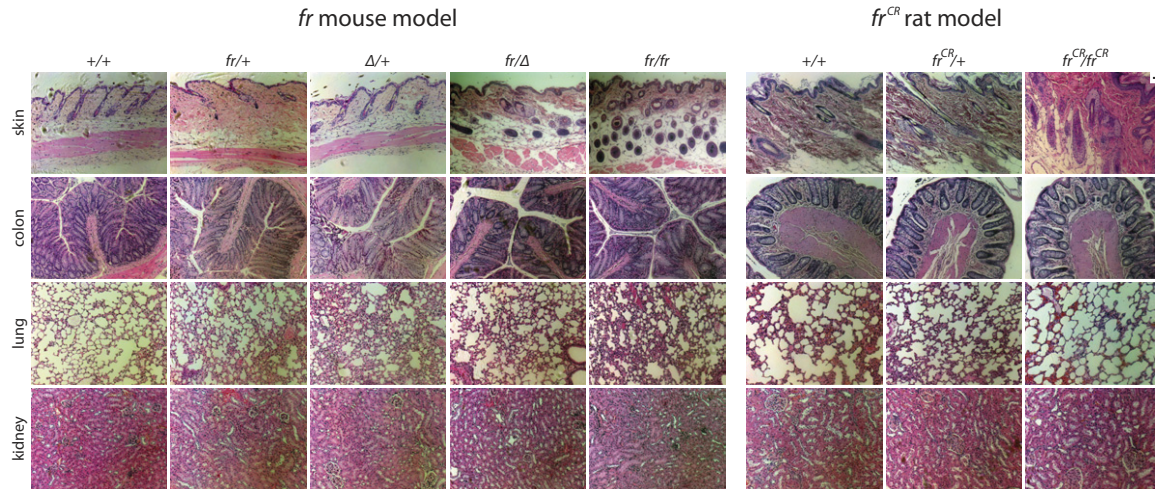


Figure 3. H&E staining of skin, colon, lung, and intestine in *fr* mouse (+/+, *fr*/+, Δ /+, *fr*/ Δ , *fr*/*fr*) and *fr*^{CR} rat (+/+, *fr*^{CR}/+, *fr*^{CR}/*fr*^{CR}) variants, performed in young-adult animals. Scale bar = 20 μ m.

did not differ from that of WT animals (Figure 4A). Analogous analyses in the skin of *fr*^{CR}/*fr*^{CR} mutant rats compared with WTs revealed a significant twofold increase in the mRNA expression of *CAP1/Prss8*. In contrast, *CAP1/Prss8* was significantly reduced in the distal colon (Figure 4B), whereas no significant changes were observed among the different genotypes in lung and kidney.

Finally, we performed Western blot analyses using CAP1/Prss8 antibody on kidney, lung, and AEC extracts from *fr* mice and *fr*^{CR} rats, respectively. CAP1/Prss8 detection in *fr*/ Δ and *fr*/*fr* mice evidenced a preferential core-glycosylated state of the mutant protein compared with the WT (Figure 4C). CAP1/Prss8 detection in *fr*^{CR}/*fr*^{CR} rats evidenced a preferential fully glycosylated state compared with controls (Figure 4D). These data are entirely in accordance with the results obtained *in vitro*.

Reduced Body Weight and Dehydration Defects in *fr*^{CR}/*fr*^{CR} Rats

fr/*fr* and *fr*/ Δ mouse mutants did not present differences in body weight compared with controls (Figure 5A). *fr*^{CR}/*fr*^{CR} rats appeared smaller and exhibited a significantly lower body weight compared with WT and heterozygous littermates (Figure 5B). To investigate whether the macroscopical and histologic defects in *fr*/*fr*, *fr*/ Δ , and *fr*^{CR}/*fr*^{CR} mutants were accompanied by functional abnormalities of the skin and to explore the ability of this organ to protect the body against excessive dehydration, we measured the TEWL. *fr*/*fr* and *fr*/ Δ mouse mutants did not differ from controls with respect to the TEWL (Figure 5C). In contrast, *fr*^{CR}/*fr*^{CR} rats exhibited a significant increase in the TEWL, suggesting that the skin barrier is compromised in these animals (Figure 5D). Moreover, *fr*^{CR}/*fr*^{CR} rats presented diarrhea accompanied by increased stool hydration (Figure 5, E and F).

Significantly Decreased ENaC Activity in the Distal Colon of *fr*/*fr*, *fr*/ Δ , and *fr*^{CR}/*fr*^{CR} Animals

CAP1/Prss8 can increase ENaC-mediated sodium currents.^{6,31} To investigate the effect of CAP1/Prss8 V170D and G54-P57 deletion mutations on ENaC activity *in vivo*, the amiloride-sensitive rectal PD was measured in the distal aspect of the colon of both *fr* mouse and *fr*^{CR} rat animal models. Because amiloride is a specific and potent inhibitor of ENaC,³³ the amiloride-sensitive PD is an indirect indicator of ENaC function. Rectal PD in rodents follows circadian variation, reflecting differential metabolic activity of the animals during the day.³⁴ We therefore performed *in vivo* measurements in the morning and afternoon of two different days. Δ /+ and *fr*/+ heterozygotes did not manifest differences compared with the WTs. *fr*/*fr* and *fr*/ Δ mice revealed a significant decrease in the amiloride-sensitive PD, reflecting a significantly reduced ENaC activity in the distal aspect of the colon (Figure 6A). Just as *fr*/*fr* and *fr*/ Δ mice did, *fr*^{CR}/*fr*^{CR} rats demonstrated a significant less negative PD. Surprisingly, *fr*^{CR}/+ heterozygous rats had a reduced PD only in the morning, whereas in the afternoon the values were not different from WTs (Figure 6B).

Discussion

We examined whether the spontaneous V170D and G54-P57 deletion mutations within the *CAP1/Prss8* gene of *fr* mice and *fr*^{CR} rats, respectively, may cause their skin phenotypes and have additional consequences on the homeostasis of various organs where CAP1/Prss8 is expressed. *In silico* experiments indicated that the mutation V170D may alter CAP1/Prss8 protein structure because of unfavorable interactions of hydrophobic side chains with polar Asp, and, most likely, the change of V170 to Asp would lead a more severe modification of the three-dimensional configuration than the 2.4-Kcal loss of energy upon mutation to Ala. G54-P57 residues in CAP1/

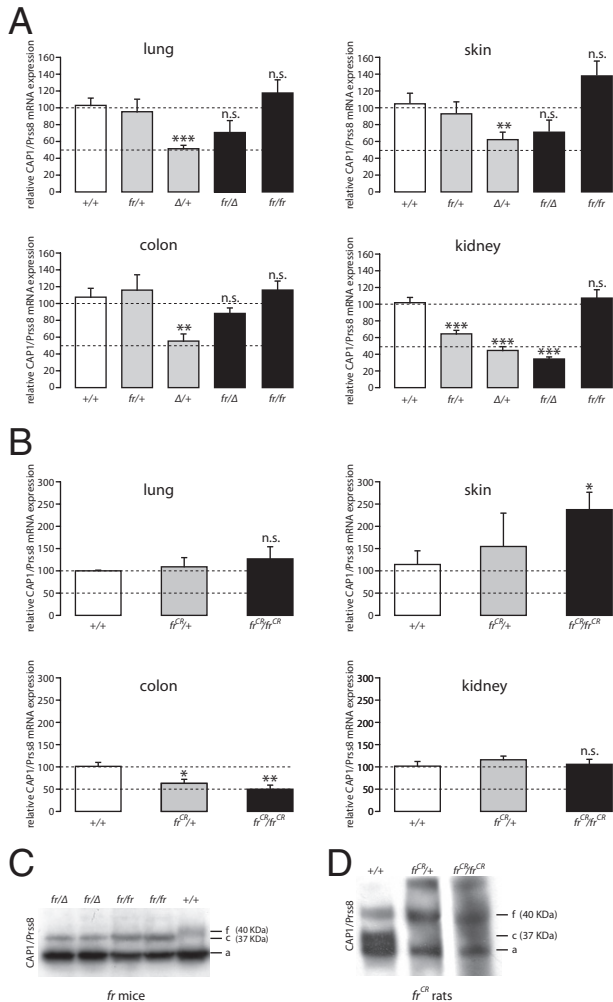


Figure 4. **A:** *CAP1/Prss8* mRNA levels, relative to β -actin, investigated by quantitative real-time PCR in the lung, skin, colon, and kidney of *fr* mice (+/+ $n = 10$; *fr*+/+ $n = 6$; Δ /+ $n = 8$; *fr*/ Δ $n = 4$; *fr*/*fr* $n = 9$ number of analyzed animals). **B:** *CAP1/Prss8* mRNA levels, relative to β -actin, investigated by quantitative real-time PCR, in the lung, skin, colon, and kidney of *fr*^{CR} rats (+/+ $n = 4$; *fr*^{CR}/+ $n = 4$; *fr*^{CR}/*fr*^{CR} $n = 4$ number of analyzed animals). * $P < 0.05$, ** $P < 0.01$, *** $P < 0.001$. **C:** Western blot analysis performed on kidney extracts from *fr* mice using CAP1/Prss8 antibody. f, fully glycosylated; c, core glycosylated; a, aspecific band. Analogous results were obtained from lung extracts. Three animals per genotype were analyzed. **D:** Western blot analysis using CAP1/Prss8 antibody performed on lung AECs isolated from *fr*^{CR} rats. Two animals per genotype were analyzed.

Prss8 resulted in solvent exposed, and their deletion could have a considerable impact on folding and architecture of the protein. These alterations of the protein structure may modify the interaction of CAP1/Prss8 with its effectors. We and other researchers have demonstrated that CAP1/Prss8 can increase the activity of the epithelial sodium channel ENaC in various expression systems^{8,31,35}, therefore, CAP1/Prss8 activity can be evaluated by measuring ENaC currents. When we injected CAP1/Prss8 V170D and G54-P57 deletion mutants in the *Xenopus* oocytes, we observed that these mutations do not prevent the expression of the protein at the plasma membrane and their capability to activate the channel when co-expressed. However, the ability of CAP1/Prss8 V170D and G54-P57 deletion mutants to stimulate ENaC appeared significantly decreased. West-

ern blot analyses and pulse-chase experiments revealed a differential glycosylation state of the two mutant proteins compared with the WT CAP1/Prss8, evidencing a preferential core glycosylated state of the V170D mutant versus a preferential fully glycosylated state of the G54-P57 deletion mutant, indicating an increased retention of the V170D mutant in the endoplasmic reticulum and enhanced intracellular transport of the G54-P57 deletion mutant. In addition to the changes in the glycosylation state, pulse-chase experiments demonstrated that the degradation and thus the stability of the mutant proteins do not change compared with the WT. However, a significant amount of energy lost upon mutation of V170 and W56 to Ala is found by *in silico* alanine scanning. This loss of energy might modify the three-dimensional conformation of the mutant proteins that may be responsible of a differential glycosylation state and eventually reduce their activity.

To determine the role of CAP1/Prss8 in the different tissues, we previously deleted the mouse CAP1/Prss8 gene locus, located on chromosome 7, in a temporally and/or tissue-specific manner¹⁹ and revealed crucial roles for this serine protease at least in the skin and lung.^{7,6,1} *fr*/*fr* mice, *fr*/ Δ mice, and *fr*^{CR}/*fr*^{CR} rats displayed a significant reduction in the embryonic viability compared with the expected mendelian inheritance, coinciding with the prenatal lethality of the CAP1/Prss8 knockout

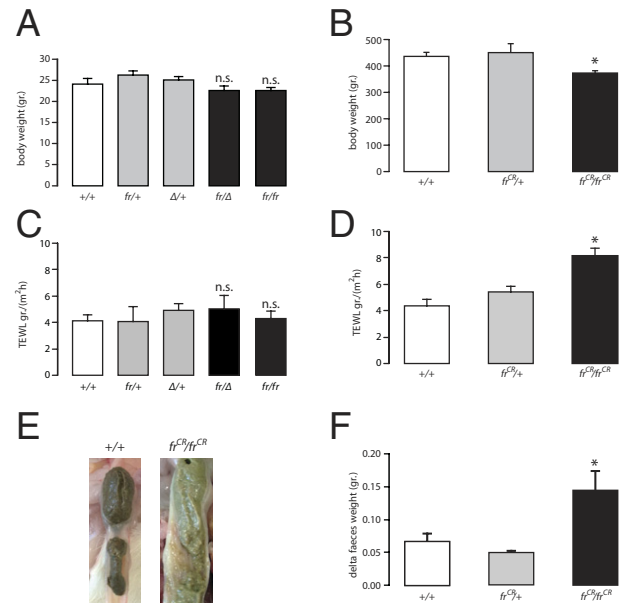


Figure 5. **A:** Body weight measurements expressed in grams of *fr* mice (+/+ $n = 12$; *fr*+/+ $n = 15$; Δ /+ $n = 23$; *fr*/ Δ $n = 13$; *fr*/*fr* $n = 22$ number of analyzed animals), performed in young adult animals. n.s., nonsignificant. **B:** Body weight measurements expressed in grams of *fr*^{CR} rats (+/+ $n = 8$; *fr*^{CR}/+ $n = 8$; *fr*^{CR}/*fr*^{CR} $n = 10$; *** $P < 0.001$, male rats only), performed in young adult animals. Same results were obtained for female rats (+/+ 283 ± 6.2 $n = 6$; *fr*^{CR}/+ 296 ± 6.6 $n = 7$; *fr*^{CR}/*fr*^{CR} 259 ± 12.1 $n = 4$; $P < 0.05$). **C:** TEWL measurements of *fr* mice (+/+ $n = 10$; *fr*+/+ $n = 5$; Δ /+ $n = 8$; *fr*/ Δ $n = 5$; *fr*/*fr* $n = 9$) expressed in grams on square meters per hour. **D:** TEWL measurements of *fr*^{CR} rats (+/+ $n = 4$; *fr*^{CR}/+ $n = 4$; *fr*^{CR}/*fr*^{CR} $n = 4$; * $P < 0.05$) expressed in grams on square meters per hour. **E:** Representative pictures of the intestinal content of *fr*^{CR}/*fr*^{CR} and WT rats clearly show an increased liquid content in the stools of the *fr*^{CR}/*fr*^{CR} mutants. **F:** Feces water content, assessed as difference between freshly collected and completely dehydrated stools (+/+ $n = 6$; *fr*^{CR}/+ $n = 3$; *fr*^{CR}/*fr*^{CR} $n = 7$; * $P < 0.05$).

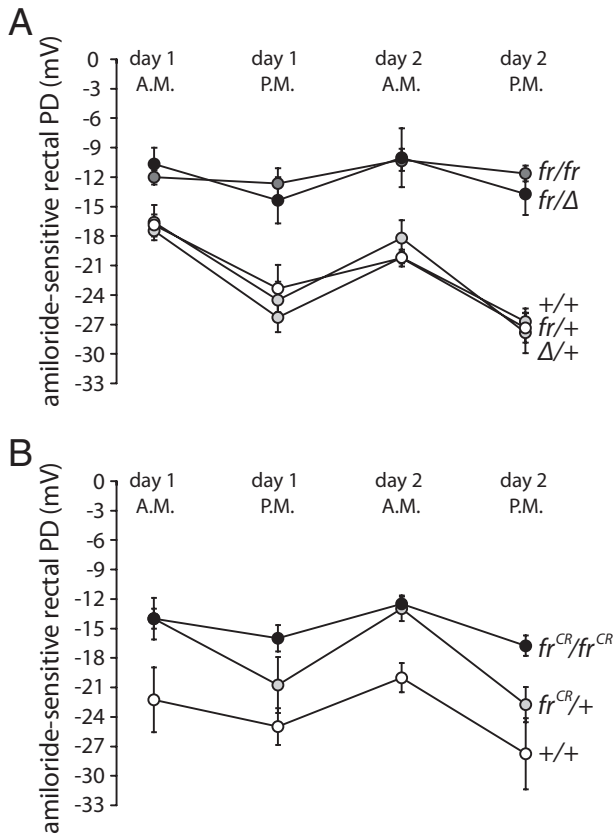


Figure 6. A: Amiloride-sensitive rectal PD, reflecting ENaC activity and expressed in millivolts, measured in the distal colon of *fr* mice (+/+, $n = 12$; *fr/fr* $n = 12$; Δ/Δ $n = 13$; *fr/Δ* $n = 10$; *fr/fr* $n = 10$) (+/+ versus *fr/fr*, $P < 0.05$; +/+ versus *fr/Δ*, $P < 0.01$). **B:** Amiloride-sensitive rectal PD, reflecting ENaC activity and expressed in millivolts, measured in the distal colon of *fr^{CR}* rats (+/+ $n = 4$; *fr^{CR}/+* $n = 4$; *fr^{CR}/fr^{CR}* $n = 4$). Measurements were performed both in the morning and in the afternoon of two different days (day 1 and day 2) (+/+ versus *fr^{CR}/fr^{CR}*, $P < 0.05$).

mice and strongly indicating a pleiotropic role of CAP1/Prss8 in embryonic development. Of interest, similar histopathologic alterations occurred in the skin of *fr/fr*, *fr/Δ*, and *fr^{CR}/fr^{CR}* animals, denoting that both mouse and rat skin structure is sensitive to CAP1/Prss8 mutations and altered function. Skin anomalies in frizzy and hairless animals did not appear to be accompanied by inflammation; thus, these defects might originate during embryonic development and hair morphogenesis. Interestingly, *fr^{CR}/fr^{CR}* rats exhibited, in addition to alopecia and hyperkeratosis, an increase in the size and number of sebaceous glands. Sebum is a mixture of lipids³⁶ that coat the fur as a hydrophobic protection against dehydration and for heat insulation,³⁷ and *fr^{CR}/fr^{CR}* animals may compensate their excess in loss of water through the skin by increasing the production of sebum.

The *fr* mutation first appeared in 1949 at the Jackson Laboratory and was identified in 1951 by Falconer and Snell³⁸ on a mixed genetic background that included the genetically linked recessive visible markers pink-eyed dilution (*p*), chinchilla (*Tyrch*), and shaker-1 (*Myo7a*). We consider unlikely that those or other additional mutations in *fr/fr* animals could contribute to the phenotype because the same phenotype is maintained or even en-

hanced in the *fr/Δ* animals and absent in the heterozygotes. In contrast, we cannot exclude the implications of additional recessive mutations on the phenotype of *fr^{CR}/fr^{CR}* rats, and a complementation test could solve this issue, but so far CAP1/Prss8 knockout alleles in rats are not available. Additional mutations in *fr^{CR}/fr^{CR}* animals could be responsible for the baldness and permeability defects observed in the skin and intestine of mutant rats but not in *fr/fr* and *fr/Δ* mice. Alternatively, baldness and permeability defects in *fr^{CR}/fr^{CR}* rats could be the result of more severe consequences generated by the CAP1/Prss8 G54-P57 deletion mutation compared with the CAP1/Prss8 V170D mutation or might be species dependent.

Although decreased in the distal colon, CAP1/Prss8 transcription levels increased in the skin of *fr^{CR}/fr^{CR}* rats, and a tendency for CAP1/Prss8 mRNA levels to augment could also be noticed in *fr/Δ* mice, not only in the skin but also in the colon and lung. These data reveal a different transcriptional regulation of mutated CAP1/Prss8 in different organs and a transcriptional up-regulation of mutated CAP1/Prss8 in *fr/Δ* mice that might be due to compensatory effects.

Dehydration defects, caused by either skin or intestine anomalies, are often accompanied by body weight loss.^{39,40} Both skin-specific CAP1/Prss8 knockout and CAP1/Prss8 overexpressing mice presented increased skin dehydration accompanied by loss in body weight,^{7,1} and the tight junction functionality was defective in the skin-specific CAP1/Prss8 knockouts.⁷ Similarly, *fr^{CR}/fr^{CR}* rats showed significant reduction in body weight and manifested increased loss of water through the skin and intestine, evidencing epidermal permeability barrier defects that might be due to an effect of mutant CAP1/Prss8 on tight junctions and/or on sodium and therefore water reabsorption. ENaC activity was significantly reduced in the distal colon of mutant mice and rats, and this decrease occurred at the same extent as that observed in intestine-specific CAP1/Prss8 knockout mice (data not shown). These data indicate that *fr/fr* and *fr/Δ* animals exhibit the same reduction in the basal activity of ENaC as that of CAP1/Prss8 loss-of-function mutants.

The three subunits of ENaC are expressed by surface epithelial cells of the distal colon,⁴¹ and several serine proteases that activate ENaC *in vitro* are also expressed in the gastrointestinal tract, with a tissue distribution broader than that of ENaC. CAP1/Prss8 is present in the stomach and colon in rats and in the stomach, small intestine, and distal colon in mice.^{35,31} The activity of ENaC depends on more than one serine protease, and we have previously shown that the serine protease CAP3/matriptase is able to increase ENaC currents from sixfold to 10-fold.³¹ It is noteworthy that both skin-specific deletion of CAP1/Prss8 and complete abrogation of CAP3/matriptase in mice caused leaky skin barrier^{42,7} and that intestine-specific deletion of CAP3/matriptase provoked colon enlargement, persistent diarrhea, and increased intestinal paracellular permeability.⁴³ Moreover, CAP1/Prss8 and CAP3/matriptase are constitutively co-localized in most epithelia⁴⁴ and have been proposed to be involved in the same proteolytic cascade.^{11,45} Thus, it is

presumable that CAP1/Prss8 and CAP3/Tmprss14 cooperate to maintain the homeostasis of different organs.

In conclusion, the present study shows that both *fr* mouse and *fr^{CR}* rat models share similar features, such as reduced embryonic viability, abnormal allocation of hair follicles in the dermis, and reduced amiloride-sensitive sodium current in the distal colon. Together these data support that *fr* and *fr^{CR}* are mutant alleles of the *CAP1/Prss8* gene. *fr* and *fr^{CR}* therefore appear as suitable models for *CAP1/Prss8* decreased function in the whole organism, and the consequences of mutated *CAP1/Prss8* on its effectors and related pathways will be the object of further research.

Acknowledgments

We thank Dr. Thomas R. King (New Britain, CT) for kindly providing the *fr* and *fr^{CR}* animal models, Profs. Kaethi Geering and Bernard C. Rossier for helpful suggestions and critical reading of the manuscript, and all of the members of the Hummler Laboratory for discussions. We also thank Dr. Dominique Marchant for technical assistance with the Western blot on isolated AEC extracts. We are grateful to the Mouse Pathology platform and the Cellular Imaging Facility platform, University of Lausanne.

References

1. Frateschi S, Camerer E, Crisante G, Rieser S, Membrez M, Charles RP, Beermann F, Stehle JC, Breiden B, Sandhoff K, Rotman S, Haftek M, Wilson A, Ryser S, Steinhoff M, Coughlin SR, Hummler E: PAR2 absence completely rescues inflammation and ichthyosis caused by altered CAP1/Prss8 expression in mouse skin. *Nature Commun* 2011, 2:161
2. Puente XS, Sanchez LM, Overall CM, Lopez-Otin C: Human and mouse proteases: a comparative genomic approach. *Nature Rev* 2003, 4:544–558
3. Puente XS, Sanchez LM, Gutierrez-Fernandez A, Velasco G, Lopez-Otin C: A genomic view of the complexity of mammalian proteolytic systems. *Biochem Soc Trans* 2005, 33:331–334
4. Rawlings ND, Morton FR, Kok CY, Kong J, Barrett AJ: MEROPS: the peptidase database. *Nucleic Acids Res* 2008, 36:D320–325
5. Verghese GM, Tong ZY, Bhagwandin V, Caughey GH: Mouse prostaticin gene structure, promoter analysis, and restricted expression in lung and kidney. *Am J Respir Cell Mol Biol* 2004, 30:519–529
6. Planes C, Randrianarison NH, Charles RP, Frateschi S, Cluzeaud F, Vuagniaux G, Soler P, Clerici C, Rossier BC, Hummler E: ENaC-mediated alveolar fluid clearance and lung fluid balance depend on the channel-activating protease 1. *EMBO Mol Med* 2009, 2:26–37
7. Leyvraz C, Charles RP, Rubera I, Guitard M, Rotman S, Breiden B, Sandhoff K, Hummler E: The epidermal barrier function is dependent on the serine protease CAP1/Prss8. *J Cell Biol* 2005, 170:487–496
8. Vallet V, Chraïbi A, Gaeggeler HP, Horisberger JD, Rossier BC: An epithelial serine protease activates the amiloride-sensitive sodium channel. *Nature* 1997, 389:607–610
9. Vuagniaux G, Vallet V, Jaeger NF, Hummler E, Rossier BC: Synergistic activation of ENaC by three membrane-bound channel-activating serine proteases (mCAP1, mCAP2, and mCAP3) and serum- and glucocorticoid-regulated kinase (Sgk1) in *Xenopus* oocytes. *J Gen Physiol* 2002, 120:191–201
10. Nariyoshi T, Kitamura K, Adachi M, Miyoshi T, Iwashita K, Shiraishi N, Nonoguchi H, Chen LM, Chai KX, Chao J, Tomita K: Regulation of prostasin by aldosterone in the kidney. *J Clin Invest* 2002, 109:401–408
11. Camerer E, Barker A, Duong DN, Ganesan R, Kataoka H, Cornelissen I, Darragh MR, Hussain A, Zheng YW, Srinivasan Y, Brown C, Xu SM, Regard JB, Lin CY, Craik CS, Kirchhofer D, Coughlin SR: Local protease signaling contributes to neural tube closure in the mouse embryo. *Dev Cell* 2010, 18:25–38
12. Takahashi SS, Inaguma S, Ikeda Y, Cho Y-M, Hayashi N, Inoue T, Sugimura Y, Nishiyama N, Fujita T, Chao J, Ushijima T, Shirai T: Down-regulated expression of prostasin in high-grade or hormone-refractory human prostate cancers. *Prostate* 2003, 54:187–193
13. Chen LM, Chai KX: Prostasin serine protease inhibits breast cancer invasiveness and is transcriptionally regulated by promoter DNA methylation. *Int J Cancer* 2002, 97:323–329
14. Sakashita K, Mimori K, Tanaka F, Tahara K, Inoue H, Sawada T, Ohira M, Hirakawa K, Mori M: Clinical significance of low expression of Prostasin mRNA in human gastric cancer. *J Surg Oncol* 2008, 98: 559–564
15. Mok SC, Chao J, Skates S, Wong K-k, Yiu GK, Muto MG, Berkowitz RS, Cramer DW: Prostasin, a potential serum marker for ovarian cancer: identification through microarray technology. *J Natl Cancer Inst* 2001, 93:1458–1464
16. Spacek DV, Perez AF, Ferranti KM, Wu LK, Moy DM, Magnan DR, King TR: The mouse frizzy (*fr*) and rat 'hairless' (*fr^{CR}*) mutations are natural variants of protease serine S1 family member 8 (*Prss8*). *Exp Dermatol* 2010, 19:527–532
17. Paul EL, Badal R, Thompson DS, Magnan DR, Soucy FM, Khan IM, Houghton RA, King TR: The mouse frizzy mutation (*fr*) maps between D7Csu5 and D7Mit165. *Exp Dermatol* 2008, 17:640–644
18. Panteleyev AA, Christiano AM: The Charles River "hairless" rat mutation is distinct from the hairless mouse alleles. *Comp Med* 2001, 51:49–55
19. Rubera I, Meier E, Vuagniaux G, Merillat AM, Beermann F, Rossier BC, Hummler E: A conditional allele at the mouse channel activating protease 1 (*Prss8*) gene locus. *Genesis* 2002, 32:173–176
20. Ahearn K, Akkouris G, Berry PR, Chrissluis RR, Crooks IM, Dull AK, Grable S, Jeruzal J, Lanza J, Lavoie C, Maloney RA, Pitruzzello M, Sharma R, Stoklasek TA, Tweeddale J, King TR: The Charles River "hairless" rat mutation maps to chromosome 1: allelic with fuzzy and a likely orthologue of mouse frizzy. *J Hered* 2002, 93:210–213
21. Hinz U: From protein sequences to 3D-structures and beyond: the example of the UniProt knowledgebase. *Cell Mol Life Sci* 2010, 67: 1049–1064
22. Rickert KW, Kelley P, Byrne NJ, Diehl RE, Hall DL, Montalvo AM, Reid JC, Shipman JM, Thomas BW, Munshi SK, Darke PL, Su HP: Structure of human prostasin, a target for the regulation of hypertension. *J Biol Chem* 2008, 283:34864–34872
23. Eswar N, Webb B, Marti-Renom MA, Madhusudhan MS, Eramian D, Shen MY, Pieper U, Sali A: Comparative protein structure modeling using MODELLER. *Curr Protoc Protein Sci* 2007, Chapter 2:Unit 2.9
24. Melo F, Feytmans E: Assessing protein structures with a non-local atomic interaction energy. *J Mol Biol* 1998, 277:1141–1152
25. Schymkowitz J, Borg J, Stricher F, Nys R, Rousseau F, Serrano L: The FoldX web server: an online force field. *Nucleic Acids Res* 2005, 33:W382–W388
26. Puoti A, May A, Rossier BC, Horisberger JD: Novel isoforms of the beta and gamma subunits of the *Xenopus* epithelial Na channel provide information about the amiloride binding site and extracellular sodium sensing. *Proc Natl Acad Sci U S A* 1997, 94:5949–5954
27. Geering K, Theulaz I, Verrey F, Hauptle MT, Rossier BC: A role for the beta-subunit in the expression of functional Na⁺-K⁺-ATPase in *Xenopus* oocytes. *Am J Physiol* 1989, 257:C851–C858
28. Planes C, Leyvraz C, Uchida T, Angelova MA, Vuagniaux G, Hummler E, Matthay M, Clerici C, Rossier B: In vitro and in vivo regulation of transepithelial lung alveolar sodium transport by serine proteases. *Am J Physiol Lung Cell Mol Physiol* 2005, 288:L1099–L1109
29. Geering K, Beggah A, Good P, Girardet S, Roy S, Schaefer D, Jaunin P: Oligomerization and maturation of Na,K-ATPase: functional interaction of the cytoplasmic NH2 terminus of the beta subunit with the alpha subunit. *J Cell Biol* 1996, 133:1193–1204
30. Spraggon G, Hornsby M, Shipway A, Tully DC, Bursulaya B, Danahay H, Harris JL, Lesley SA: Active site conformational changes of prostasin provide a new mechanism of protease regulation by divalent cations. *Protein Sci* 2009, 18:1081–1094
31. Vuagniaux G, Vallet V, Jaeger NF, Pfister C, Bens M, Farman N, Courtois-Coutry N, Vandewalle A, Rossier BC, Hummler E: Activation of the amiloride-sensitive epithelial sodium channel by the serine protease mCAP1 expressed in a mouse cortical collecting duct cell line. *J Am Soc Nephrol* 2000, 11:828–834
32. Caldwell RA, Boucher RC, Stutts MJ: Serine protease activation of near-silent epithelial Na⁺ channels. *Am J Physiol Cell Physiol* 2004, 286:C190–C194

33. Loffing J, Kaissling B: Sodium and calcium transport pathways along the mammalian distal nephron: from rabbit to human. *Am J Physiol Renal Physiol* 2003, 284:F628–F643
34. Wang Q, Horisberger JD, Maillard M, Brunner HR, Rossier BC, Burnier M: Salt- and angiotensin II-dependent variations in amiloride-sensitive rectal potential difference in mice. *Clin Exp Pharmacol Physiol* 2000, 27:60–66
35. Adachi M, Kitamura K, Miyoshi T, Narikiyo T, Iwashita K, Shiraishi N, Nonoguchi H, Tomita K: Activation of epithelial sodium channels by prostasin in *Xenopus* oocytes. *J Am Soc Nephrol* 2001, 12: 1114–1121
36. Nikkari T: Comparative chemistry of sebum. *J Invest Dermatol* 1974, 62:257–267
37. Strauss JS, Pochi PE, Downing DT: The sebaceous glands: twenty-five years of progress. *J Invest Dermatol* 1976, 67:90–97
38. Falconer DS, Snell GD: Two new hair mutants, rough and frizzy in the house mouse. *J Hered.* 1952, pp. 53–57
39. Herrmann T, van der Hoeven F, Grone HJ, Stewart AF, Langbein L, Kaiser I, Liebisch G, Gosch I, Buchkremer F, Drobnik W, Schmitz G, Stremmel W: Mice with targeted disruption of the fatty acid transport protein 4 (*Fatp 4*, *Slc27a4*) gene show features of lethal restrictive dermopathy. *J Cell Biol* 2003, 161:1105–1115
40. Koletzko S, Osterrieder S: Acute infectious diarrhea in children. *Dtsch Arztebl Int* 2009, 106:539–547; quiz 548
41. Canessa CM, Merillat AM, Rossier BC: Membrane topology of the epithelial sodium channel in intact cells. *Am J Physiol* 1994, 267:C1682–C1690
42. List K, Haudenschild CC, Szabo R, Chen W, Wahl SM, Swaim W, Engelholm LH, Behrendt N, Bugge TH: Matriptase/MT-SP1 is required for postnatal survival, epidermal barrier function, hair follicle development, and thymic homeostasis. *Oncogene* 2002, 21:3765–3779
43. List K, Kosa P, Szabo R, Bey AL, Wang CB, Molinolo A, Bugge TH: Epithelial integrity is maintained by a matriptase-dependent proteolytic pathway. *Am J Pathol* 2009, 175:1453–1463
44. List K, Hobson JP, Molinolo A, Bugge TH: Co-localization of the channel activating protease prostasin/(CAP1/PRSS8) with its candidate activator, matriptase. *J Cell Physiol* 2007, 213:237–245
45. Netzel-Arnett S, Currie BM, Szabo R, Lin C-Y, Chen L-M, Chai KX, Antalis TM, Bugge TH, List K: Evidence for a matriptase-prostasin proteolytic cascade regulating terminal epidermal differentiation. *J Biol Chem* 2006, 281:32941–32945